



1                   **Sensitivity of instrumental line shape with respect to**  
2                   **different optical attenuators and resulting error propagation**  
3                   **into atmospheric trace gas retrievals**

4                   Y. W. Sun<sup>1)+</sup>, M. Palm<sup>2)+</sup>, C. Weinzierl<sup>2)</sup>, C. Petri<sup>2)</sup>, J. Notholt<sup>2)</sup>,  
5                   Y. T. Wang<sup>2)</sup> and C. Liu<sup>3,4,1)\*</sup>

6                   (1 *Key Lab. of Environmental Optics and Technology, Anhui Institute of Optics and*  
7                   *Fine Mechanics, Chinese Academy of Sciences, Hefei 230031, China*)

8                   (2 *University of Bremen, Institute of Environmental Physics, P. O. Box 330440,*  
9                   *28334 Bremen, Germany*)

10                  (3 *University of Science and Technology of China, Hefei, 230026, China*)

11                  (4 *Center for Excellence in Urban Atmospheric Environment, Institute of Urban*  
12                  *Environment, Chinese Academy of Sciences, Xiamen 361021, China*)

13                  +These two authors contributed equally to this work

14                  **Abstract:** The TCCON (Total Carbon Column Observing Network) and most  
15                  NDACC (Network for Detection of Atmospheric Composition Change) assume an  
16                  ideal ILS (Instrumental line shape) in spectra retrieval and insert an attenuator or  
17                  select a smaller entrance aperture to take some intensities away if incident radiation is  
18                  too strong. These processes may alter the alignment of a high resolution FTIR  
19                  (Fourier transform infrared) spectrometer and may result in biases due to ILS drift. In  
20                  this paper, we first investigated the sensitivity of ILS monitoring with respect to  
21                  various typical optical attenuators for ground-based high resolution FTIR  
22                  spectrometers within the TCCON and NDACC networks. Both lamp and sun cell  
23                  measurements were conducted in this analysis via the insertion of five different  
24                  attenuators before and behind the interferometer. We compared the HCl profile  
25                  retrievals using an ideal ILS with those using an actual measured ILS. The results  
26                  showed that the total column amounts were under-estimated by about 0.4% if the ME  
27                  (modulation efficiency) amplitude deviates by about -3.5%. Furthermore, the retrieval  
28                  errors increased and the obvious profile deviations are shown in a height range with a  
29                  high retrieval sensitivity. ILSs deduced from all scenarios of lamp cell measurements

---

Correspondence to: C. Liu ([chliu81@ustc.edu.cn](mailto:chliu81@ustc.edu.cn))



30 were compared, and were further used to derive the HCl profile from the same  
31 spectrum. As a result, the disturbances to the ILS of a high resolution FTIR  
32 spectrometer with respect to inserting different attenuators before and behind the  
33 interferometer are quantified. The resulting ILS errors propagation into gas retrievals  
34 were also analyzed. In conclusion, the alignment of the optical parts before the  
35 interferometer is more critical than those behind the interferometer, and the entrance  
36 aperture (the focus of the entrance parabolic/spherical mirror) exhibited the most  
37 critical influence. An optimum method to adapt the incident intensity of a detector  
38 was finally deduced.

39 **Key words:** TCCON, NDACC, FTIR, Instrumental Line Shape

## 40 **1 Introduction**

41 High resolution direct solar Fourier transform infrared (FTIR) spectrometry is the  
42 most precise ground-based remote sensing technique used in deriving the  
43 column-average abundance of greenhouse gases (GHGs) or mixing ratio profiles of  
44 many other trace gases (Wunch et al., 2010 and 2011; Washenfelder, 2006;  
45 Messerschmidt et al., 2010; Kurylo, 1991; Davis et al., 2001). Currently, both the two  
46 well-established operational observation networks, i.e., NDACC (Network for  
47 Detection of Atmospheric Composition Change, <http://www.ndacc.org/>) and TCCON  
48 (Total Carbon Column Observing Network, <http://www.tcon.caltech.edu/>), use high  
49 resolution FTIR spectrometers to record direct sun spectra. Both networks have  
50 operated internationally more than ten years and their results are widely used in  
51 atmospheric physics and chemistry (Angelbratt et al., 2011; Wunch et al., 2010 and  
52 2011; Washenfelder, 2006; Messerschmidt et al., 2010). The NDACC started  
53 operation in 1991 and mainly works in mid-infrared (MIR) spectral range of 750 to  
54  $4200\text{ cm}^{-1}$  (Kurylo, 1991; Schneider, et al., 2008; Kohlhepp et al., 2011; Hannigan et  
55 al., 2009; Wang et al., 2015). These spectra are used to retrieve time series of mixing  
56 ratio profiles for  $\text{O}_3$ ,  $\text{HNO}_3$ , HCl, HF, CO,  $\text{N}_2\text{O}$ ,  $\text{CH}_4$ , HCN,  $\text{C}_2\text{H}_6$ ,  $\text{ClONO}_2$   
57 (Schneider et al., 2008; Sussmann, et al., 2011) and other gases, e.g.,  $\text{H}_2\text{O}$  (Notholt, et  
58 al., 1994; Palm et al., 2010),  $\text{H}_2\text{O}/\text{HDO}$  ratio (Schneider et al., 2006), OCS (Notholt, et



59 al., 2003; Wang, et al., 2016) or NH<sub>3</sub> (Dammers et al., 2015). In contrast, the TCCON  
60 started operation in 2004 and provides highly precise and accurate column-average  
61 abundance for CO<sub>2</sub>, CH<sub>4</sub>, N<sub>2</sub>O, HF, CO, H<sub>2</sub>O and HDO derived from near infrared  
62 (NIR) spectra (Hase et al., 2012 and 2013; Wunch et al., 2011; Keppel-Aleks, et al.,  
63 2011; Warneke, et al., 2010). In order to achieve consistent results between different  
64 FTIR sites, the TCCON and NDACC have developed strict data acquisition and  
65 retrieval methods for minimizing the site to site differences (Hase et al., 2012;  
66 <http://www.ndacc.org/>; <http://www.tcon.caltech.edu/>). Interferograms are acquired  
67 with similar instruments operated with common detectors, acquisition electronics  
68 and/or optical filters. Typically, NDACC and TCCON FTIR spectrometers are the  
69 high-resolution 125HR, 120HR, 125M or 120M manufactured by Bruker Optics,  
70 Germany<sup>†</sup> (<http://www.ndacc.org/>; <http://www.tcon.caltech.edu/>; <https://www.bruker.com/>). These interferograms were first converted to spectra and later to  
72 retrieved products using dedicated processing algorithms, i.e., GFIT, PROFFIT or  
73 SFIT (Hase et al., 2006; Dohe et al., 2013; Griffith, et al., 2010). However, biases  
74 between sites may arise due to the behavior of individual spectrometers, if not  
75 properly characterized. Some of these differences result from a misalignment of an  
76 interferometer, which can change abruptly as a consequence of operator intervention  
77 or drift slowly due to mechanical degradation over time (Hase et al., 2012; Miller et  
78 al., 2007; Olsen et al., 2004). This misalignment effects can be diagnosed by the  
79 variations of instrumental line shape (ILS) (Hase et al., 1999 and 2001). It has become  
80 a part of FTIR network practice to regularly use a low-pressure calibration gas cell  
81 (HBr or HCl) to diagnose a misalignment of the spectrometer and to improve the  
82 alignment when indicated (Wunch et al., 2010; Hase et al., 1999 and 2001). A  
83 successful alignment scheme for high resolution spectrometers was proposed about a  
84 decade ago and has become the standard alignment procedure for both TCCON and  
85 NDACC (Hase et al., 2001). As a result, the individual systematic errors and site to  
86 site biases caused by misalignment due to mechanical degradation were already

<sup>†</sup> NOTE: In the TCCON network, only the Bruker HR series instruments are used. In the NDACC network, other instruments are used as well, e.g. the Bruker M series, a BOMEM in Toronto, Canada and a self built in Pasadena, USA.



87 minimized.

88 Typically, alignment procedure is performed by using a specific optical scenario,  
89 e.g., a specified source, aperture, beam splitter, filter and detector (Hase et al.,2001).  
90 The TCCON and most NDACC assume an ideal ILS in spectra retrieval. In order to  
91 adapt the intensity of the incident radiation, an attenuator is inserted in the light path  
92 (TCCON network<sup>‡</sup>) or a different entrance aperture is selected. These processes may  
93 alter the specified alignment of a high resolution FTIR spectrometer and result in  
94 biases due to ILS drift. An alternative way which does not alter the alignment of a  
95 spectrometer is selecting a suitable amplifier gain depending on incoming intensities.  
96 However, this method's contribution is limited and may be plagued with deteriorating  
97 SNR (signal to noise ratio) of the spectrum. Currently, the degree of ILS changes  
98 caused by the above processes and resulting error propagation into spectra retrievals  
99 are still not fully quantified. Furthermore, if the actual ILS is left undetermined and  
100 simply assumed to be perfect, a substantial systematic error might be introduced in the  
101 retrieval. In this paper, we designed experiments to investigate the sensitivity of ILS  
102 monitoring for ground-based high resolution FTIR spectrometer with respect to  
103 different optical attenuators. This paper also analyzed how ILS changes affect the gas  
104 retrievals, due to the insertion of various attenuators. Resultantly, we propose the  
105 optimum optical attenuation method. First, we describe the experiments design and  
106 procedures performed for this study in detail. Secondly, we present the optical  
107 background removal for both lamp and sun cell measurements. Thirdly, we analyzed  
108 the propagation of an error in the ILS into TCCON and NDACC retrieval.  
109 Furthermore, we compared the ILSs deduced from all scenarios of lamp cell  
110 measurements, and used them to derive HCl profile from the same spectrum. As a  
111 result, the disturbances of different attenuators to the ILS of a high resolution FTIR  
112 spectrometer and resulting errors propagation into gas retrievals are quantified.  
113 Following the uncertainty's estimation and discussion, this paper closes with a  
114 summary.

---

<sup>‡</sup> The attenuation is left constant and is the same for all instruments because the aperture has strong influence on the instrumental line shape.



## 115 **2 Experimental design**

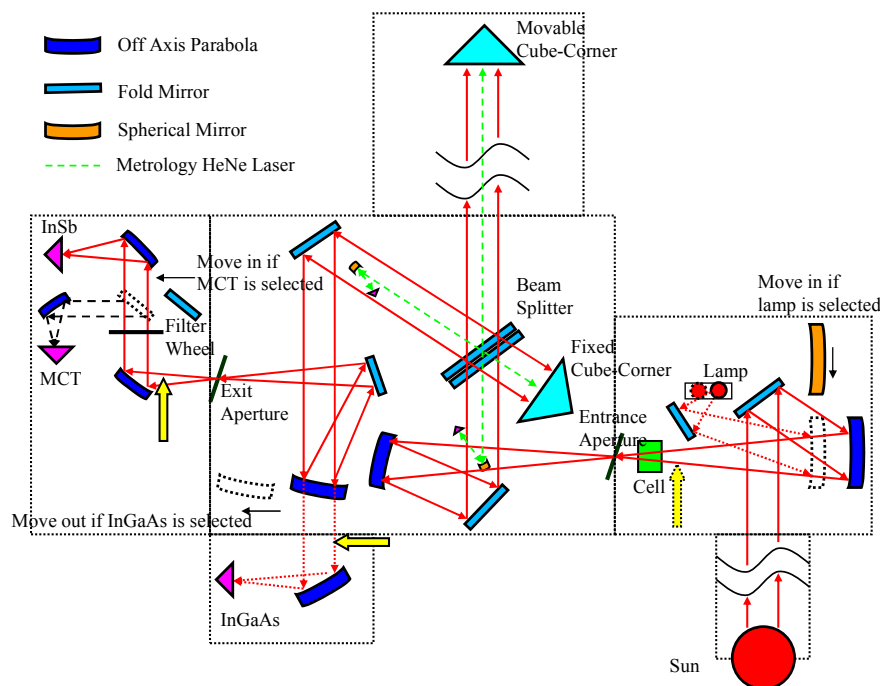
116 All experiments were performed with a Bruker FTS 125HR located in Bremen,  
117 Germany. This instrument is operated by Institute of Environmental Physics (IUP),  
118 University of Bremen, Germany, and it is part of the networks NDACC and TCCON  
119 since 2004 (Messerschmidt et al., 2010). The instrument's alignment was regularly  
120 checked with the 1mm entrance aperture, CaF<sub>2</sub> or KBr beam splitter, InGaAs or InSb  
121 detector using the HCl and HBr gas cells, respectively. The functional layout of the  
122 experimental setup is shown in Fig. 1(a).

123 Five different kinds of attenuators (Fig. 1(b)) were used in the experiments.  
124 Attenuator #1 is a flat metal perforated on a regular grid. Attenuator #2 restricts the  
125 diameter of a beam. Attenuator #3 blocks the opposite 1/4 pairs of a beam and lets the  
126 rest 1/4 pairs pass through. Attenuator #4 blocks half of a beam. Attenuator #5 is a 0.8  
127 mm or 1.2mm aperture located in the entrance aperture wheel. We performed two  
128 groups of experiments within three weeks. The alignment during these experiments  
129 was not changed and was assumed to be constant. This was backed by experience,  
130 which showed that, ILS changes only slowly if ambient conditions are stable. The  
131 group one experiments inserted an attenuator behind the interferometer, i.e., in the  
132 detector compartment. The group two experiments inserted an attenuator before the  
133 interferometer, i.e., in the source compartment (see Fig.1(a)). Each group experiment  
134 was made up of 8 individual measurement scenarios. For each individual scenario, we  
135 inserted only one attenuator and selected either the internal lamp or external sun as the  
136 light source. The internal lamps for NDACC and TCCON ILS monitoring are Globar  
137 and Tungsten, respectively. All sun cell measurements were performed within one day  
138 with a clear sky condition suitable for observations. The KBr beam splitter, a filter  
139 with CWN (center wave number) of 2300cm<sup>-1</sup> and FWHM (Full Width at Half  
140 Maximum) of 500cm<sup>-1</sup>, and the InSb detector were selected in NDACC ILS  
141 monitoring. While the TCCON ILS monitoring used the CaF<sub>2</sub> beam splitter and the  
142 InGaAs detector. In group one experiment, attenuator #1~4 was inserted to a specified  
143 place just before the exit parabolic mirror. In group two experiment, attenuator #1~4



144 was inserted to a specified place between the entrance parabolic/spherical mirror and  
145 its focus (i.e., the selected entrance aperture). While attenuator #5, i.e. an entrance  
146 aperture different from the default 1mm aperture, is right in the focal plane of the  
147 entrance parabolic/spherical mirror (see Fig.1(a)). In this manner, the attenuator #5 is  
148 in the image of the light source for both TCCON and NDACC. The group one and  
149 group two experiments for TCCON were in the parallel beam and in the divergent  
150 beam, respectively. While both experiments for NDACC were in the divergent beam  
151 (see Fig.1(a)). NDACC ILS monitoring uses a HBr cell of 2cm length filled with 2  
152 mbar of HBr. TCCON ILS monitoring uses 10 cm long cells filled with 5 mbar of HCl.  
153 The HBr and HCl cells were provided by the National Center for Atmospheric  
154 Research (NCAR, Boulder, Colorado, USA) and Caltech (Washenfelder, 2006),  
155 respectively. Both of them were calibrated by Hase (Hase et al., 2013) at the KIT  
156 Karlsruhe, Germany. We performed 60 and 6 times of repeat measurement for each  
157 TCCON ILS monitoring scenario using the internal lamp and the sun, respectively.  
158 The repeat measurement for NDACC were set at 50 and 4 times, respectively. The  
159 repeated times in sun ILS monitoring, were much less than the lamp ILS monitoring,  
160 because, non-negligible error would have arisen if the atmosphere was assumed to be  
161 stable for a longer period.

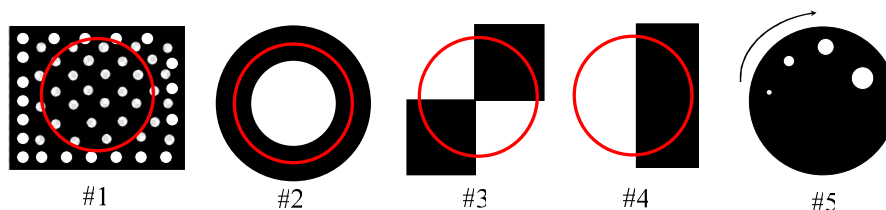
162 The LINEFIT software is used for the ILS calculation. It retrieves a complex  
163 modulation efficiency (ME) as a function of optical path difference (OPD), which is  
164 represented by a ME amplitude and a ME phase error (Hase et al., 1999). The ME  
165 amplitude is referred to the width of the ILS while the ME phase error quantifies the  
166 degree of ILS asymmetry. If the spectrometer meets the ideal nominal ILS  
167 characteristics, the ME amplitude would be unity, and the ME phase error would be  
168 zero along the whole interferogram. Further details are provided by Hase (2012). For  
169 comparison, the standard micro window (WM) mode rather than broadband mode  
170 were used for all ILSs retrieval and all spectra were normalized to the same level  
171 before analysis. The WM mode facilitates the background removal especially in sun  
172 cell measurements.



173

174

(a)



175

176

(b)

177 Fig. 1. Functional layout of the experimental setup, (a) the sketch of the whole optical path  
 178 and (b) five different attenuators. The yellow arrows in (a) show the place where the attenuators  
 179 #1~4 are inserted. In detail: the solid yellow arrows are for the classical group one experiments,  
 180 i.e., attenuator #1~4 was inserted to a specified place just before the exit parabolic mirror. The  
 181 dotted yellow arrow is for the group two experiments, i.e., attenuator #1~4 was inserted to a  
 182 specified place between the entrance parabolic/spherical mirror and its focus (i.e., the selected  
 183 entrance aperture). While attenuator #5 is right in the focal plane of the entrance  
 184 parabolic/spherical mirror. The red circle in (b) indicates the size of the beam. Check the text for  
 185 the detailed descriptions of the five attenuators.

### 186 3 The optical background removal

187 Optical background is a measurement without cells inserted into the optical path.  
 188 The optical background consists of two parts. One is called the atmosphere structure,



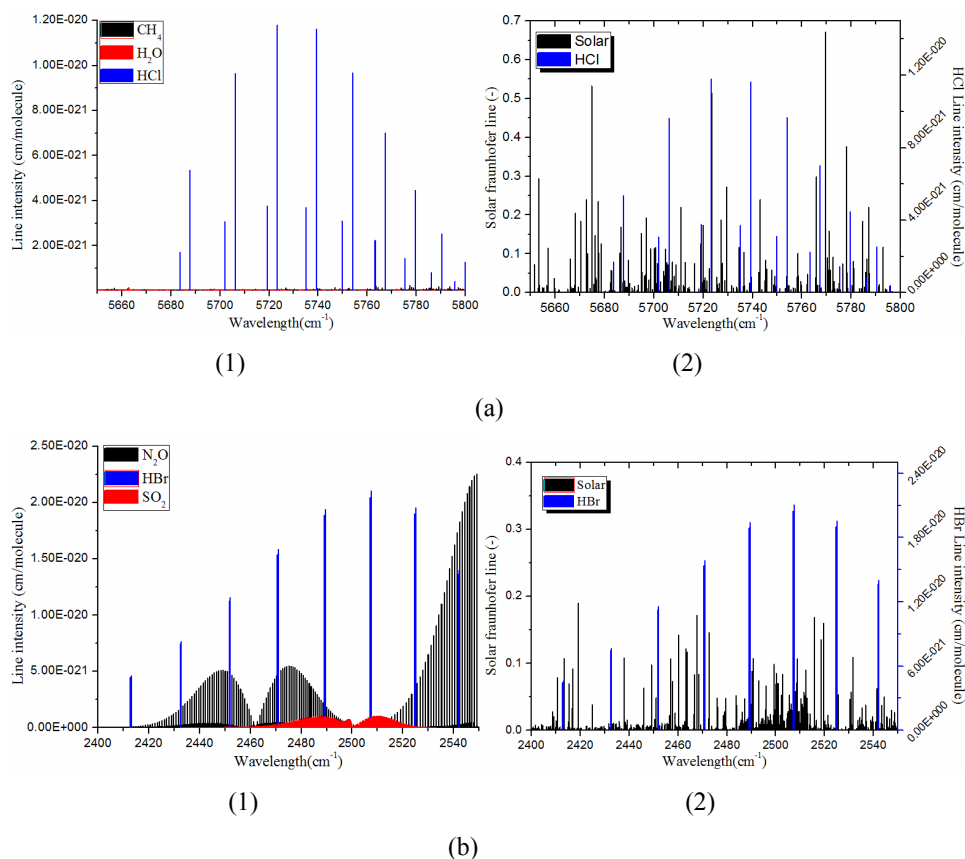
189 which is caused by the absorption of co-interfering gases and extinction of some  
190 atmospheric constituents. The other part is called system structure which is caused by  
191 the instrumental system, e.g., the light source, the filters, etc. In Fig.2 the typical  
192 interfering gases and the solar Fraunhofer lines within the HCl and HBr fitting regions  
193 are shown. In the TCCON case, H<sub>2</sub>O and CH<sub>4</sub> have non-negligible absorptions in the  
194 same region as HCl. The NDACC case is more complicated, both N<sub>2</sub>O and SO<sub>2</sub> show  
195 strong interferences in HBr region. Furthermore, non-negligible solar Fraunhofer lines  
196 within both HCl and HBr regions are shown. Therefore, optical background removal  
197 is rather important especially for the sun cell measurement. In principle, two methods  
198 can be used to remove the optical background. The first method is including all the  
199 interfering items in each fitting micro window and fit them together with the ILS. The  
200 second method is utilizing each spectrum (taken during inserting the cells) to divide  
201 by the reference spectrum (i.e., spectrum taken without cells inserted into the optical  
202 path). Since the interfering items in the solar spectrum are not easy to quantify, in this  
203 study, we used the second method to remove the optical background for both lamp  
204 and sun cell measurements.

205 We used the default optical settings scenario, i.e., "select the 1mm aperture without  
206 using any attenuators", to demonstrate the optical background removal for both lamp  
207 and sun cell measurements. Typical lamp and sun spectra used for TCCON and  
208 NDACC ILS retrievals are shown in Fig. 3. The sun cell measurements in both HCl  
209 and HBr regions exhibited more interference than the lamp cell measurements. The  
210 lamp measurements are nearly free of interference except the continuum curvature,  
211 whereas the atmospheric structures are obviously shown in sun measurements. This is  
212 attributable to the following reasons: a), the atmospheric measurement itself remains  
213 disturbed even a typical clear sky atmospheric condition is selected. b), the internal  
214 lamp spectra are nearly free of spectral structures, whereas the sun spectra are  
215 complex, the non-negligible Fraunhofer lines exist (as shown in Fig. 2). c), the optical  
216 path in sun cell measurement is much longer than the lamp cell measurement. The  
217 solar beam enforces the use of the interfering gases, resulting in more complicated  
218 interferences.

219 Fig.4 shows the fitted cases for TCCON and NDACC ILS retrievals after removing  
220 the optical background. The LINEFIT achieved good ILS fittings for both TCCON  
221 and NDACC regardless of lamp or solar spectrum. The ILS modulation efficiencies  
222 and phase errors deduced from Fig. 4 are shown in Fig.5. It concludes that the lamp



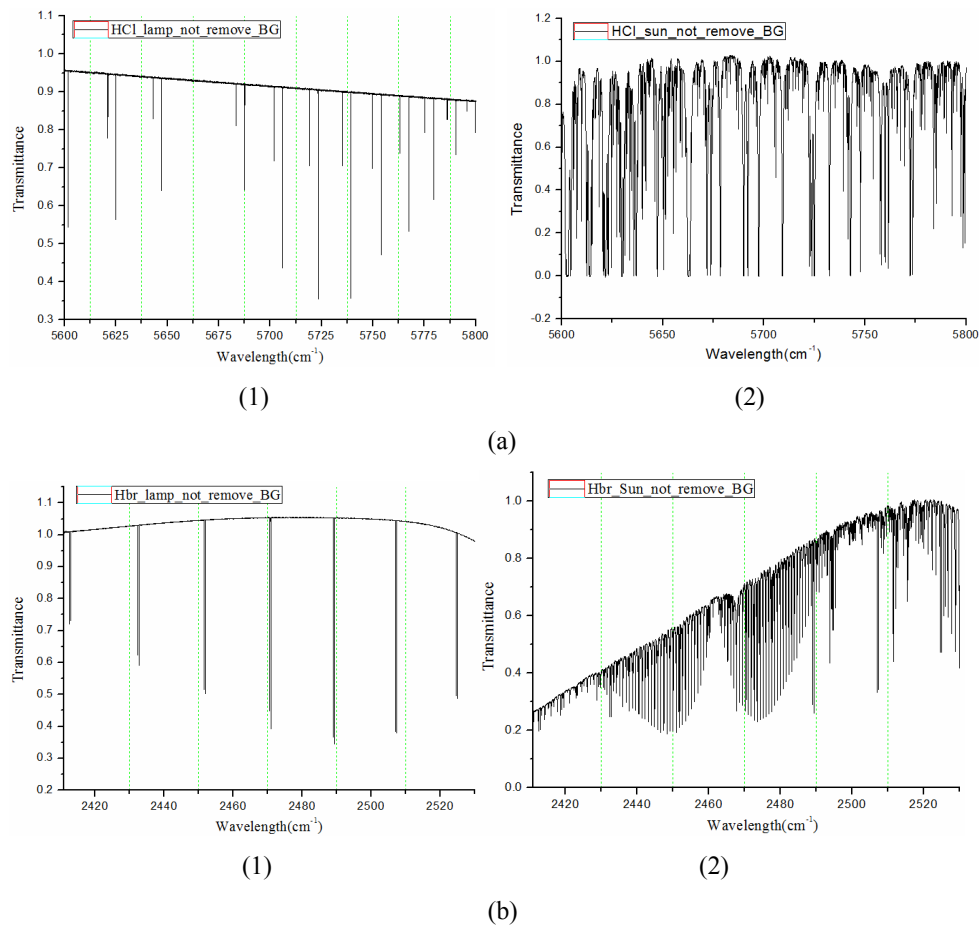
223 and solar spectrum can achieve consistent ILS retrievals for both TCCON and  
224 NDACC, though the solar spectrum is much more structured than the lamp spectrum.  
225 We also performed the similar comparison for all other individual measurement  
226 scenarios, and deduced the same conclusion.



227 Fig. 2. Typical interfering gases and the solar Fraunhofer lines within the HCl and HBr fitting  
228 regions. (a) and (b) are the cases for HCl and HBr region, respectively. (1) and (2) of each sub  
229 panel show the interfering gases and the solar Fraunhofer lines, respectively. The absorption  
230 intensities of all gases are adopted from HITRAN2008. The solar Fraunhofer lines are adopted  
231 from the input files of the TCCON software GGG2014.



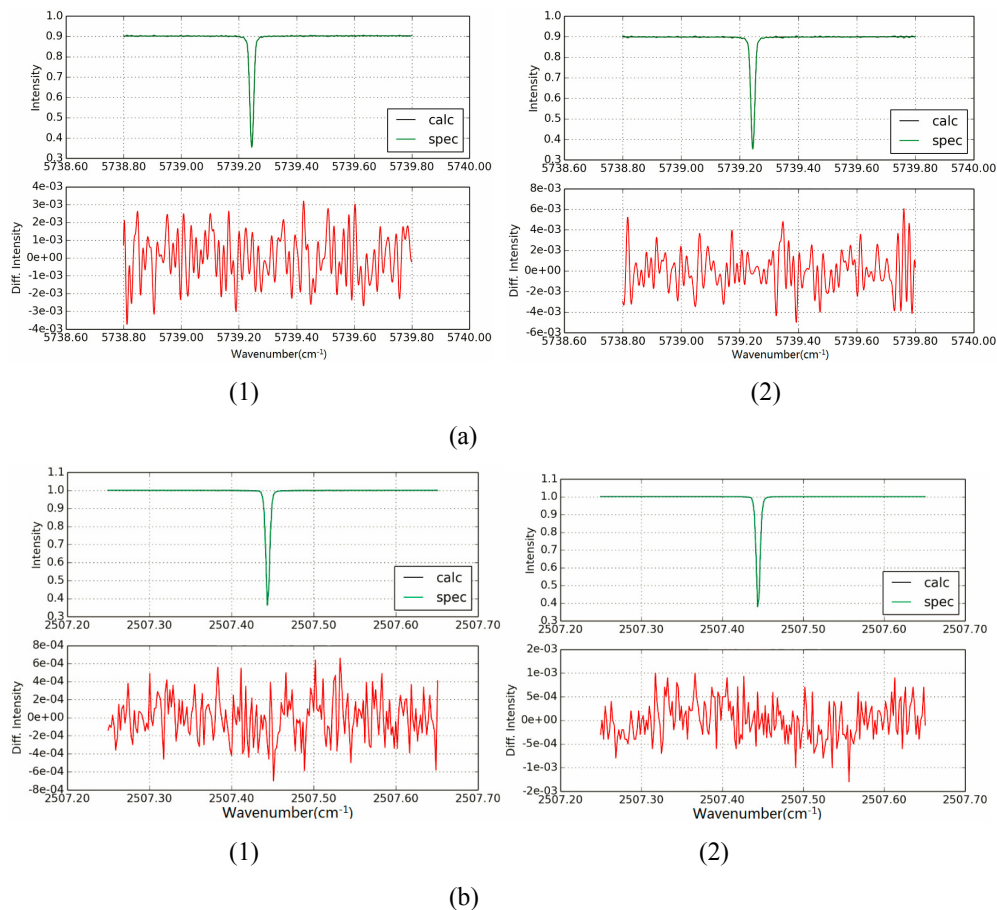
232



233 Fig. 3. The normalized spectra used for TCCON and NDACC ILS retrievals. (a) and (b) are  
234 for TCCON and NDACC ILS retrievals, respectively. (1) and (2) of each sub-plot represent lamp  
235 spectrum and solar spectrum, respectively. Less interfering structures in lamp spectra than solar  
236 spectra are shown.



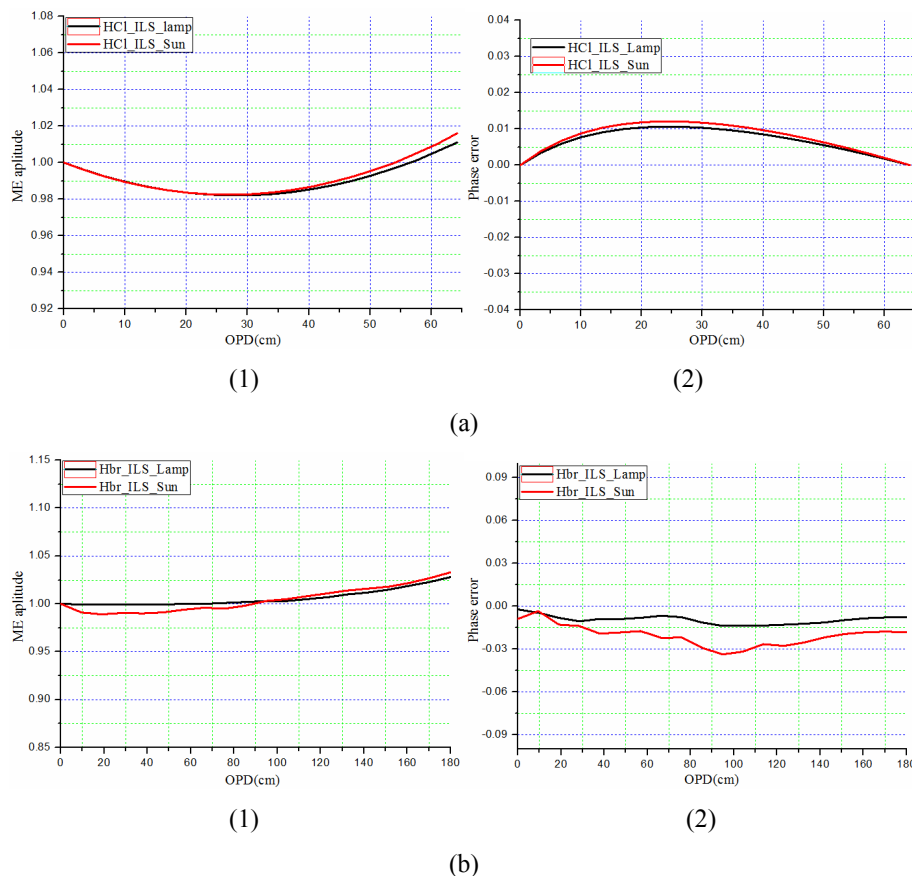
237



238 Fig. 4. The LINEFIT fitted cases for TCCON and NDACC after removing optical  
239 background. (a) and (b) are for TCCON and NDACC ILS fittings, respectively. (1) and (2) of each  
240 sub-plot represent the cases for lamp spectrum and solar spectrum, respectively. Only one  
241 micro-window for each case is shown and the residual are in most cases less than 0.2%.



242



243 Fig. 5. ILS retrievals derived from lamp (black lines) and sun spectra (red lines). (a) and (b)  
244 are comparisons for TCCON and NDACC cases, respectively. (1) and (2) of each sub-plot  
245 represent the ME amplitude and phase error, respectively.

#### 246 4 Propagation of ILS error into gas retrieval

247 Hase *et al* (2013) investigated how the column-average dry-air mole fractions of  
248 CO<sub>2</sub> (XCO<sub>2</sub>) reported by TCCON are affected by a deviation of the ME amplitude  
249 from unity. They applied a disturbance on the ME amplitude and didn't take the phase  
250 error/ILS asymmetry into account due to the quantification of spectral line asymmetry  
251 was not critically affected by the assumed width of the HCl signatures provided by the  
252 cell. As a result, the propagation of ILS width error into TCCON XCO<sub>2</sub> data was  
253 quantified. A ME amplitude change of 4% at OPD<sub>max</sub>=45cm results in XCO<sub>2</sub> error on  
254 the order of 0.035%. The target site-to-site bias for the TCCON XCO<sub>2</sub> product is 0.1%.



255 Therefore, the ILS error would be of secondary importance if the ME amplitude is  
256 kept at a level of less than 4% in accordance with TCCON requirements. We applied  
257 this empirical ILS error propagation formula for TCCON in this study.

258 The TCCON XCO<sub>2</sub> result is calculated from the ratio of CO<sub>2</sub> and O<sub>2</sub> columns  
259 derived from the same spectrum. This strategy minimizes the error propagation of  
260 various instrumental and model errors into the final retrieval because instrumental  
261 distortion affects the retrievals of both gases in the same manner and therefore cancel  
262 out partially (Hase et al., 2012 and 2013; Wunch et al., 2015) . The NDACC uses a  
263 different retrieval strategy, thus Hase's empirical ILS error propagation formula  
264 doesn't apply to NDACC profile retrieval. We investigated the sensitivity of NDACC  
265 data with respect to an error in the ILS by substituting the actual measured ILS  
266 derived from lamp cell measurement into atmospheric HCl retrieval. The HCl profile  
267 and column retrievals were performed using the algorithm SFIT4, version 0.9.4.4,  
268 jointly developed at the NCAR, Boulder, Colorado, USA, University of Bremen,  
269 Germany, University of Toronto, Canada, the Belgian Institute for Space Aeronomy  
270 (BIRA-IASB), Brussels, Belgium and others. The basic principle of SFIT4 is using an  
271 optimal estimation (OE) technique for fitting calculated-to-observed spectra (Rogers,  
272 2000, Hannigan and Coffey, 2009). We applied three micro-windows, i.e., 2727cm<sup>-1</sup>,  
273 2775cm<sup>-1</sup> and 2925 cm<sup>-1</sup>, to retrieve HCl. Retrieval results between using an ideal  
274 nominal ILS and using an actual measured ILS were compared. In this study, we did  
275 not take the errors produced by SFIT4 into account because all the inputs were exactly  
276 the same except for ILS. The errors would be the same for all scenarios. The  
277 measured ILS and its ME amplitude and phase error along a function of OPD is  
278 shown in Fig.6. The ME amplitude deviation within 180cm OPD amounts to about  
279 -3.5%. Five spectra with different zenith angles taken from 2014/03/10 to 2014/03/20  
280 are involved in the comparison.

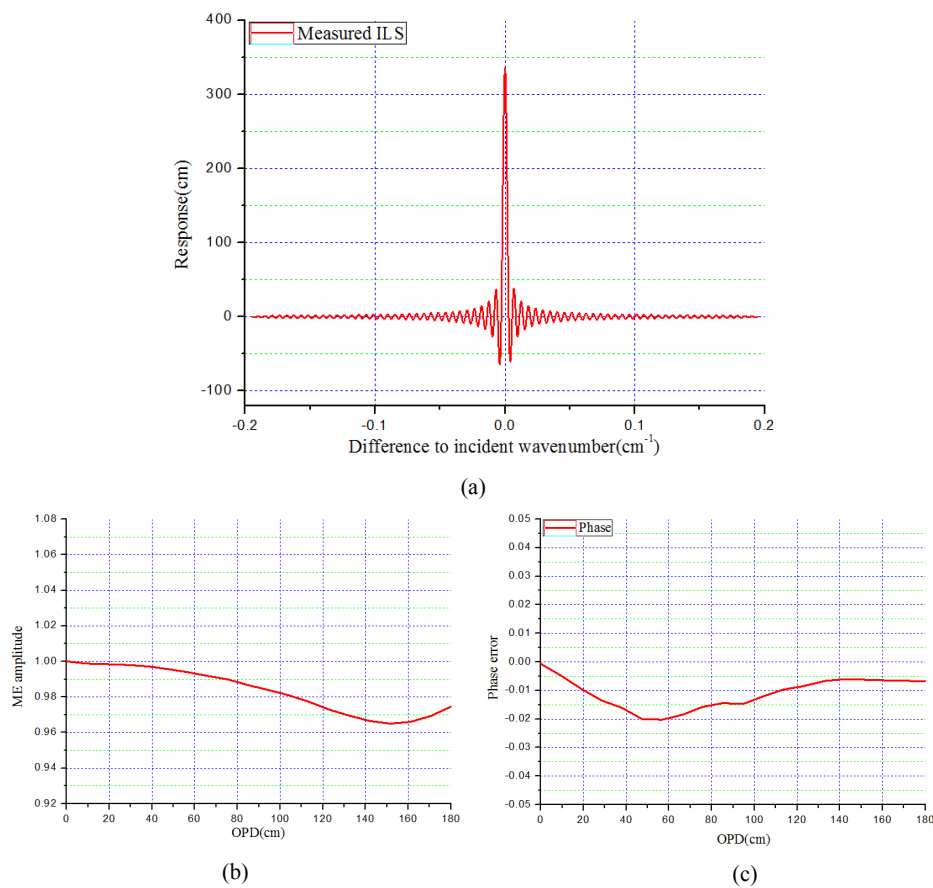
281 The comparison with respect to total column amount, total random error and total  
282 systematic error are listed in Table 1. The results show that the total column amounts  
283 were under-estimated by about 0.4% if an ideal ILS rather than an actual ILS was  
284 used. Furthermore, an error in ILS also increased both the random error and



285 systematic error. The random error and systematic error were increased by an order of  
286 0.3% to 1% and ~0.5% to 1.5%, respectively. An ILS error causes more influence on  
287 systematic error than on random error, this is probably because systematic structure is  
288 made more obvious by ILS, and a correct ILS can decrease the systematic error in the  
289 forward model calculation. The comparison with respect to HCl profile retrievals is  
290 shown in Fig.7. The retrieved HCl profiles exhibit some difference when using  
291 different ILSs and the maximum deviations lie in between 20 to 60 km. In Fig.8 the  
292 retrieval errors and averaging kernels (AK) along a function of altitude for a typical  
293 HCl profile retrieval are shown. The height range where the error statistics show more  
294 retrieval errors (Fig.8 (a)) and the averaging kernels (Fig.8 (b) and (c)) show higher  
295 retrieval sensitivities are identical to the range that the retrieved HCl profiles exhibit  
296 obvious deviations in Fig.7.



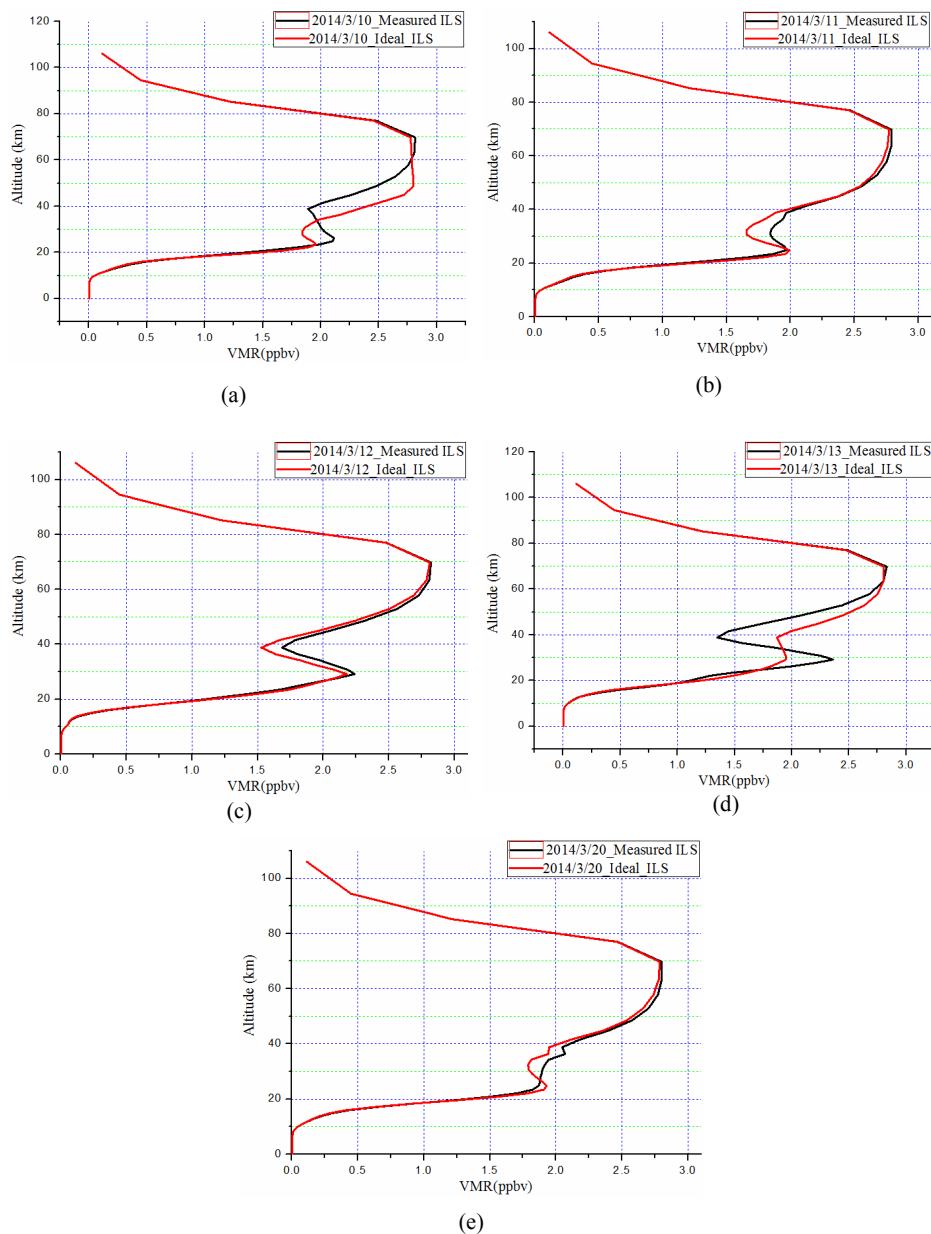
297



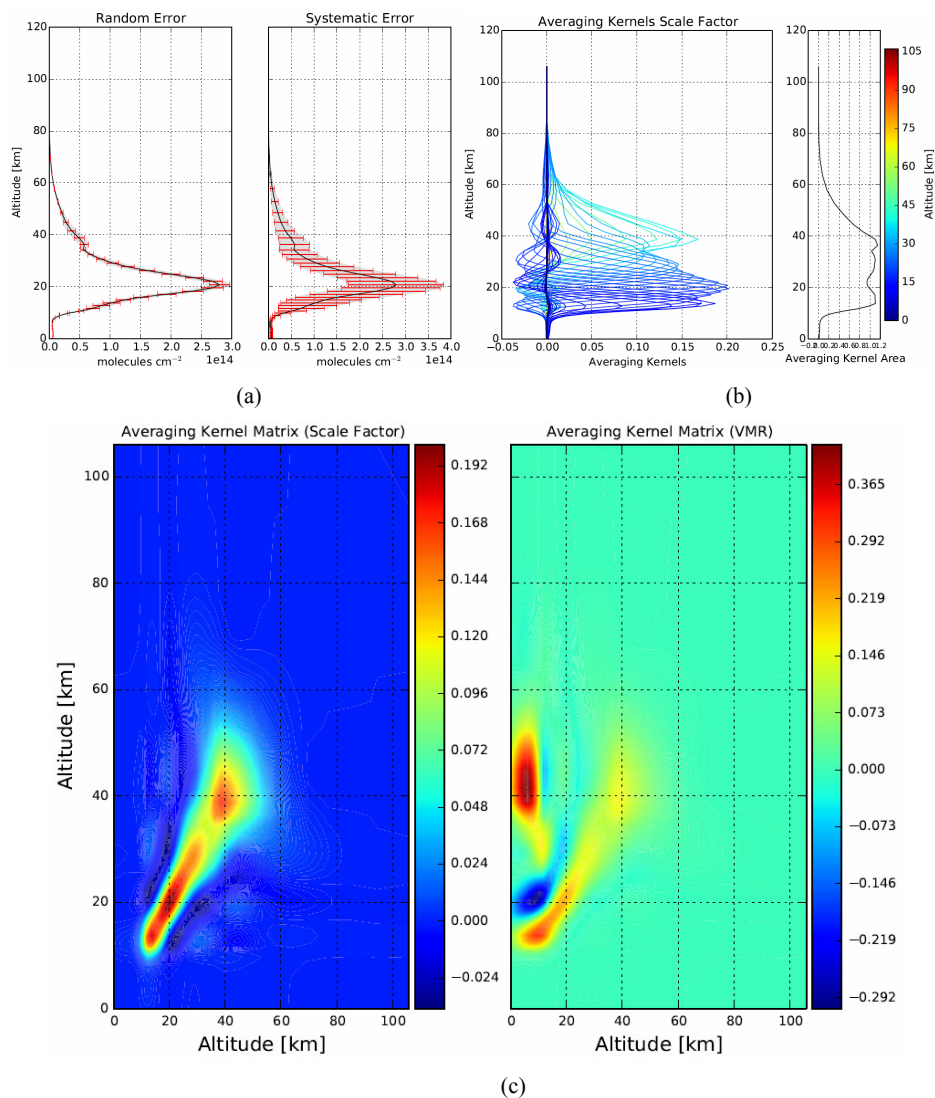
298 Fig. 6. The measured ILS used for HCl profile retrieval as well as its ME amplitude and  
299 phase error along a function of OPD. (a), (b) and (c) are the measured ILS, ME amplitude and  
300 phase error, respectively. The ILS was measured on 2014/11/20



301



302 Fig. 7. HCl profile retrievals comparison between using an ideal nominal ILS and using an  
303 ILS measured on 2014/11/20. Five spectra with different zenith angles taken from 2014/03/10 to  
304 2014/03/20 were involved. (a) to (e) are HCl profile retrievals comparison for 2014/03/10 to  
305 2014/03/13 and 2014/03/20, respectively.  
306



307 Fig. 8. Retrieval error and averaging kernels(AK) of a typical HCl profile retrieval. The  
308 spectrum was taken on 2014/03/10. (a) is a plot for the retrieval error along a function of altitude.  
309 (b) and (c) are 1D and 2D plots for the averaging kernels(AK), respectively.



Table 1 HCl retrieval results comparison between using an ideal nominal ILS and using an actual measured ILS. Five spectra with different zenith angles taken from 2014/03/10 to 2014/03/20 are involved.

Date	Solar zenith angle (°)		Total column amount (E+15 molecules*cm <sup>-2</sup> )				Total random error (%)			Total systematic error (%)		
	Measured and ideal ILS		Measured ILS	Ideal ILS	relative bias (%)	Measured ILS	Ideal ILS	relative bias (%)	Measured ILS	Ideal ILS	relative bias (%)	
2014/03/10	64.64		3.552	3.537	-0.422	0.910	0.919	+0.989	0.772	0.783	+1.425	
2014/03/11	58.38		3.242	3.228	-0.432	0.979	0.985	+0.613	0.829	0.835	+1.086	
2014/03/12	71.48		2.973	2.961	-0.404	1.016	1.019	+0.295	0.856	0.860	+0.467	
2014/03/13	74.21		3.182	3.169	-0.409	0.874	0.880	+0.686	0.746	0.753	+0.938	
2014/03/20	68.01		3.273	3.259	-0.428	0.917	0.92	+0.327	0.776	0.781	+1.03	



## 313 **5 ILS retrieval sensitivity of different attenuators**

314 The TCCON and NDACC ILS retrievals for different scenarios are presented in  
315 Fig.9 and Fig.10, respectively. The ILSs retrieved from lamp cell measurements are  
316 smoother than those retrieved from sun cell measurements for two reasons. First, we  
317 performed more times of repeat measurement for each lamp cell measurement  
318 scenario than for sun cell measurement, therefore the random noise is lower. Besides,  
319 the simpler measurement scenario makes the optical background removal of the lamp  
320 cell measurement easier and better. This is backed by Fig.4, where the fitted residual  
321 for sun spectra are relatively larger than those for lamp spectra.

322 It can be concluded that the ILS retrievals are very sensitive to various attenuators.  
323 The phase errors vary more than the ME amplitude. They indicate that the alignment  
324 of the interferometer was changed after either attenuator was inserted, and it caused  
325 more influence on optical modulation phase than optical modulation efficiency. The  
326 shift amounts of the ILS depends on the attenuator type. The ILS shifts caused by  
327 inserting attenuators #1~4 are much less than attenuator #5. Both TCCON and  
328 NDACC ILSs derived from cell measurements with inserting attenuators #1~4 are  
329 close to the ILS derived from default cell measurement scenario, with a ME amplitude  
330 change of  $< 3\%$  within  $OPD_{max}=45\text{cm}$  and  $< 6\%$  within  $OPD_{max}=180\text{cm}$ , respectively.  
331 While both TCCON and NDACC ILSs derived from cell measurements with  
332 attenuators #5 are larger than  $15\%$  at the  $OPD_{max}$ . This is most likely because the  
333 routine alignment procedure was performed by using a specified 1 mm entrance  
334 aperture, and the consistency between different apertures produce a non-negligible  
335 optical misalignment if a different aperture other than 1mm aperture was selected.  
336 This is because of mechanical inaccuracies in the mechanics of the front aperture. As  
337 the ILS asymmetry is less critical than ILS width, we set ME amplitude changes of  
338  $4\%$  within  $OPD_{max}=45\text{cm}$  and  $8\%$  within  $OPD_{max}=180\text{cm}$  as the upper thresholds  
339 for TCCON and NDACC, respectively. They amount to maximum gas retrieval biases  
340 related to ILS drift on the order of  $\sim 0.035\%$  and  $\sim 0.8\%$  for TCCON  $XCO_2$  and  
341 NDACC HCl, respectively. As a result, either of the attenuators #1~4 could



342 potentially taken to decrease the intensity when the incident radiation is too strong.  
343 Furthermore, we also verified some derivatives of attenuators #1~4 as shown in  
344 Fig.11 which are also potential solutions. While selecting a smaller (bigger) entrance  
345 aperture to decrease (increase) incoming intensities which is less than optimal since  
346 the mechanical errors of different apertures may be non-negligible and inconsistent.  
347 This may be different from one instrument to the other, hence, the mechanical  
348 consistency of each aperture is recommended to be further checked before being used.  
349 The attenuator #5 has more influence on ILS than attenuators #1 ~ 4, which also  
350 indicates that the alignment of the entrance aperture (the focus of the entrance  
351 parabolic mirror) is more critical than other optical places.

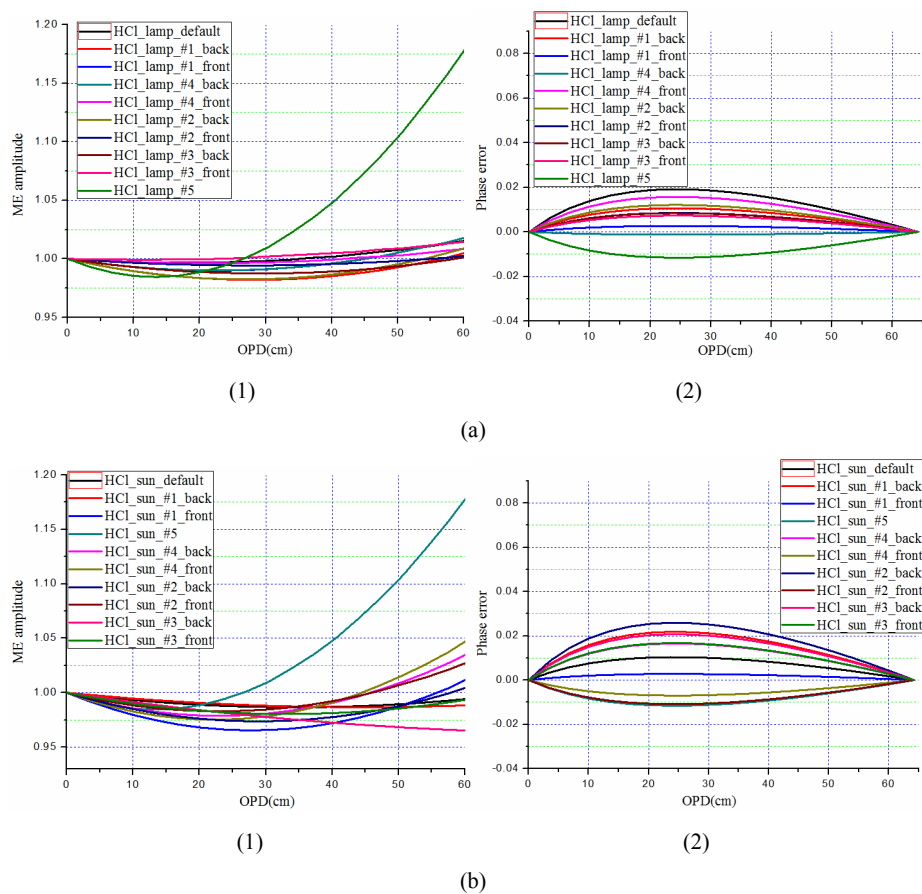
352 In order to find an optimum choice from attenuators #1 ~ 4, especially for the case  
353 that the amplifier gain of a detector can not be decreased any further, we investigated  
354 the sensitivity of NDACC data with respect to these four attenuators. ILSs derived  
355 from two groups of lamp cell measurements using attenuators #1 ~ 4 were used to  
356 retrieve atmospheric HCl, and compared with the results using an ideal ILS. Section 4  
357 shows that an error in the ILS nearly produced the same bias to all spectra. Here we  
358 only take the spectrum recorded on 2014/03/10 as an example. In contrast to section 4,  
359 here the retrieval using an ideal rather than a measured ILS was taken as the reference.  
360 In this manner, the ILSs with less biases deviated from the reference, the less ME  
361 amplitude deviated from unity and phase error deviated from zero, and the more  
362 closer to an ideal ILS assumption. The HCl total column amount retrieved by using  
363 different ILSs are listed in table 2, the total random error and total systematic error are  
364 also included. The HCl profile retrievals by using different ILSs are shown in Fig.12.  
365 The results show that both the random error and systematic error were improved a  
366 little bit by using the ILSs derived from either scenario of cell measurements. The  
367 scenarios with inserting the attenuators behind the interferometer are in most cases  
368 better than those inserting the attenuators before the interferometer. This indicates the  
369 alignment before the interferometer is more critical than that behind the interferometer.  
370 This deduction is in excellent agreement with Hase's alignment scheme (Hase, 2001).  
371 All the HCl profile retrieved via ILSs derived from cell measurements showed some  
372 deviations from the result retrieved with an ideal ILS assumption. While the result for  
373 inserting the attenuator #1 behind the interferometer exhibits the least deviation. As a



374 result, we conclude that inserting an attenuator #1 behind the interferometer is the best  
375 option. It can produce a scenario that is close to an ideal ILS assumption if the  
376 interferometer is already well aligned. On the other hand, it's not an easy task to  
377 precisely insert the attenuators #2 ~ 3 in the center of an optical path or attenuators  
378 #3~4 vertically block the optical path. Errors as this kind mainly depend on personal  
379 experience and may be different from time to time. All these technical errors would  
380 produce an error to ILS retrieval because the cross-section of the optical image  
381 passing through the interferometer is not symmetric and evenly distributed. To this  
382 point, attenuator #1 is also advantageous because it homogeneously attenuate  
383 intensities in all directions and does not have this problem.



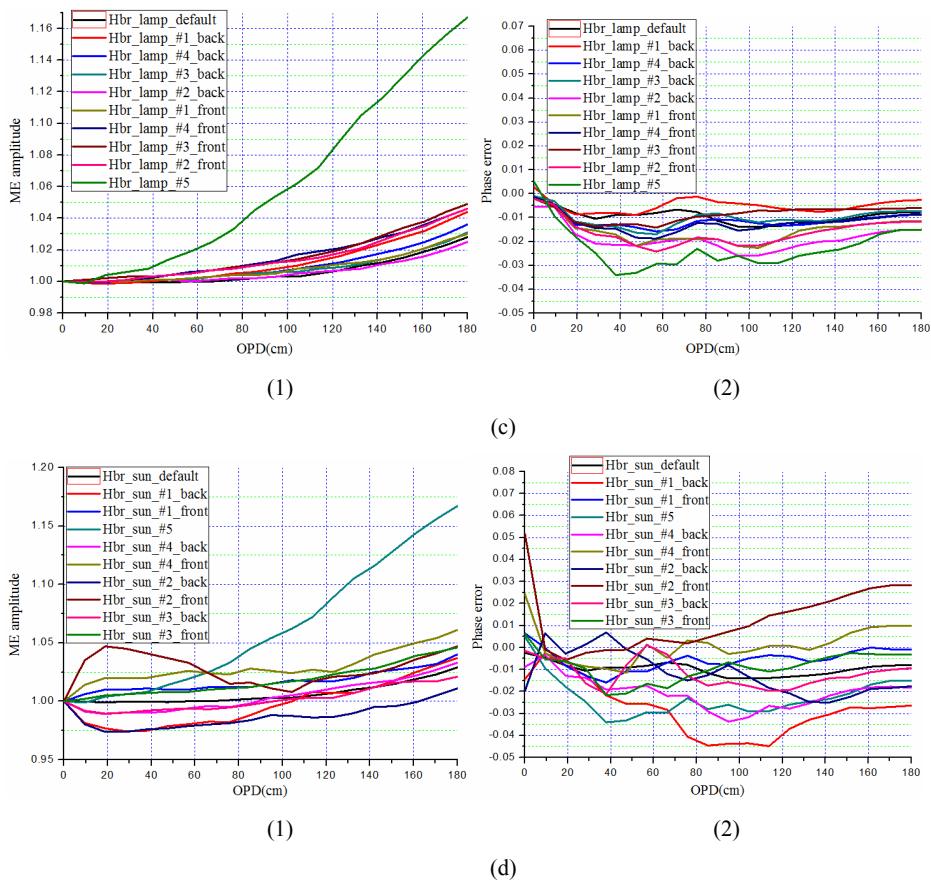
384



385 Fig. 9. TCCON ILS retrievals for different attenuators. (a) and (b) are ILS retrievals derived  
 386 from lamp and sun cell measurements, respectively. (1) and (2) of each sub-plot represent the ME  
 387 amplitude and phase error, respectively. The backgrounds in all scenarios were removed.  
 388 "HCl\_sun\_#3\_front" represents the sun HCl cell measurement performed by inserting the  
 389 attenuator #3 before the interferometer. The nomenclature for other plot labels is straightforward.



390

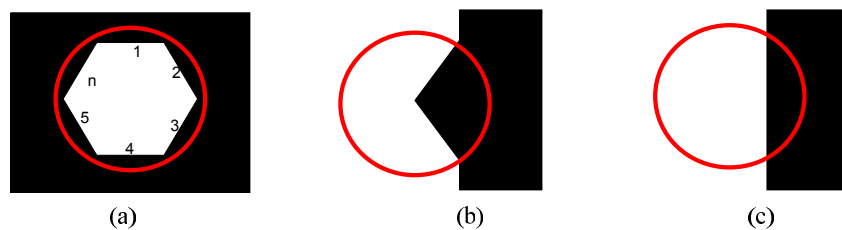


391

Fig. 10. The same as Fig.9 but for NDACC.



392



393

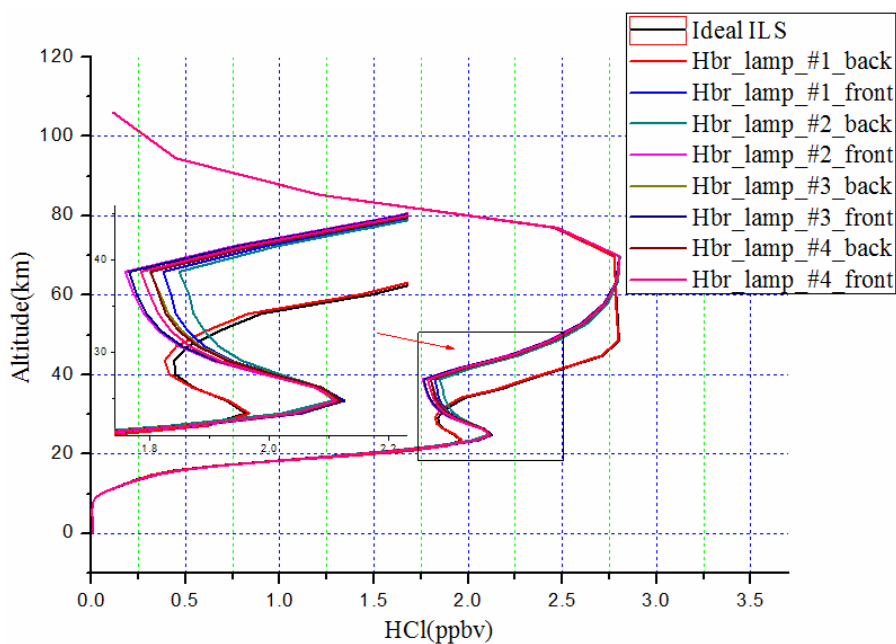
394

395

396

397

Fig. 11. Typical derivatives of attenuators #1~4 as potentials to decrease the incident intensity. (a) is a derivative of attenuator #2 which restricts the diameter of a beam with a Polygon. (b) is derivative of attenuator #3 which block a beam with an arc of Sector. (c) is a derivative of attenuator # 4 which partly blocks a beam.



398

399

400

401

402

403

404

Fig.12 HCl profile retrievals comparison between using an ideal nominal ILS and using various ILSs derived from lamp cell measurements. Spectrum saved on 2014/03/10 is taken as an example. The zoom in zone is also shown. All those HCl profile retrievals by using ILSs derived from cell measurements show some deviations from the result retrieved with an ideal ILS assumption. While the result for inserting the attenuator #1 behind the interferometer exhibits the least deviation.



Table 2 HCl retrieval results comparison between using an ideal nominal ILS and using various ILSs derived from lamp cell measurements. ILSs derived from two groups of lamp cell measurements using attenuators #1 ~ 4 were involved. Spectrum taken on 2014/03/10 is taken as an example.

Items Scenarios	Solar zenith angle (°)	Total column amount (E+15 molecules*cm <sup>-2</sup> )		Total random error (%)		Total systematic error (%)	
		values	relative bias (%)	values	relative bias (%)	values	relative bias (%)
Ideal ILS	64.64	3.537	0	0.919	0	0.783	0
HBr_lamp_#1_back	64.64	3.548	+0.311	0.918	-0.109	0.782	-0.128
HBr_lamp_#1_front	64.64	3.549	+0.339	0.912	-0.762	0.775	-1.022
HBr_lamp_#2_back	64.64	3.548	+0.311	0.913	-0.653	0.776	-0.894
HBr_lamp_#2_front	64.64	3.552	+0.424	0.911	-0.871	0.774	-1.149
HBr_lamp_#3_back	64.64	3.546	+0.254	0.913	-0.653	0.776	-0.894
HBr_lamp_#3_front	64.64	3.547	+0.283	0.912	-0.762	0.775	-1.022
HBr_lamp_#4_back	64.64	3.549	+0.339	0.912	-0.762	0.775	-1.022
HBr_lamp_#4_front	64.64	3.546	+0.254	0.913	-0.653	0.776	-0.894

405  
 406  
 407

408  
 409  
 410



## 411 **6 Uncertainties estimation and discussion**

412 One uncertainty in both sun and lamp ILS measurements arises in neglecting the  
413 alignment drifts due to mechanical degradation in all experiments. This uncertainty is  
414 of secondary importance because we performed all experiments within three weeks  
415 which was much shorter than a typical realignment interval of several months. To  
416 estimate this uncertainty, we compared the ILSs before and after all the experiments.  
417 The maximum drifts of  $\sim 2.5\%$  and  $\sim 3.6\%$  are shown for  $OPD_{\max} = 45\text{cm}$  and  $OPD_{\max}$   
418  $= 180\text{cm}$ , respectively. They amount to the deviations of ME amplitudes of  $0.0375\%$   
419 and  $0.126\%$  for TCCON and NDACC, respectively. We typically accomplished two  
420 individual lamp measurement scenarios per day and all solar measurement scenarios  
421 within one day. We assumed the mechanical degradation of the instrument varies  
422 evenly with the time. As a result for the lamp cell measurements, the effective ME  
423 drifts for each comparison set of TCCON and NDACC are  $0.00893\%$  ( $0.0375\% \cdot 5/21$ )  
424 and  $0.03\%$  ( $0.126\% \cdot 5/21$ ), respectively. They amount to the maximum gas retrieval  
425 biases of  $\sim 0.0000781\%$  and  $\sim 0.003\%$  for TCCON and NDACC data, respectively.  
426 For the sun cell measurements, all estimations are  $\sim 1/5$  of above deductions.

427 Another common uncertainty arises in errors in inputs of LINEFIT. Since we  
428 performed the same routine pro-processing procedures for all spectra and all inputs  
429 are the same except for the cell temperature. Thus, the uncertainty mainly comes from  
430 an error in a priori temperature estimation. Typically, we adjusted the a-priori  
431 temperature to find a retrieved temperature with  $\pm 2.5\text{K}$  accuracy. The scatters of the  
432 effective ME drifts (normalized to a reference temperature of  $296\text{K}$ ) are  $0.0253\%$  and  
433  $0.0591\%$  for  $OPD_{\max} = 45\text{cm}$  and  $OPD_{\max} = 180\text{cm}$ , respectively (Hase, 2013). They  
434 amount to maximum gas retrieval biases on the order of  $\sim 0.0002214\%$  and  $\sim$   
435  $0.00591\%$  for TCCON and NDACC data, respectively.

436 Assuming the atmosphere was undisturbed within the interval of each  
437 measurement scenario, would also produce uncertainties in ILS retrievals if they are  
438 derived from sun cell measurements. The clear sky condition offers relative less  
439 disturbances of aerosols, clouds and dusts, etc. Furthermore, the WM mode of



440 LINEFIT makes each fitting window to be less interfered by other atmospheric  
441 molecules. So the uncertainty would mainly come from atmospheric HCl/HBr  
442 absorption variation due to SZA deviation. For a typical measurement interval of 15  
443 minutes, a SZA deviation of  $\sim 2.5^\circ$  can normally be observed at  $SZA = 60^\circ$ . This  
444 amounts to  $\sim 8.3\%$  ( $\{[1/\cos(62.5^\circ)-1/\cos(60^\circ)]/(1/\cos(60^\circ))\}$ ) of atmospheric  
445 HCl/HBr absorption deviation. For the TCCON case, the typical atmospheric HCl  
446 total column amount as listed in table 1 is on the order of  $E+15$  molecules $\cdot\text{cm}^{-2}$ . This  
447 means the atmospheric HCl absorption deviation is on the order of  $E+14$   
448 molecules $\cdot\text{cm}^{-2}$ . While the HCl total column amount within the HCl cell is on the  
449 order of  $E+22$  molecules $\cdot\text{cm}^{-2}$  (Table 1 in Hase et al., 2013;  
450 <http://www.tcon.caltech.edu/>). Consequently, uncertainties as this kind are also  
451 negligible. A similar deduction for the NDACC case results in the same conclusion.

452 In conclusion, this study is accurate enough to resolve the ILS of each cell  
453 measurement scenario. Our study cannot identify the physical mechanisms of how the  
454 different attenuators varied the alignment of a ground-based high resolution FTIR  
455 spectrometer within the TCCON and NDACC networks, but our findings shall  
456 provide a valuable reference for all TCCON and NDACC communities because all  
457 these FTIR networks nearly operate with the same hardware and software.

## 458 **7 Summary**

459 We investigated the sensitivity of ILS monitoring for ground-based high  
460 resolution FTIR spectrometer with respect to various typical optical attenuators. We  
461 performed both lamp and sun cell measurements via the insertion of five different  
462 attenuators before and behind the interferometer to derive different ILSs. We found  
463 that both solar spectrum and the lamp spectrum can achieve consistent ILS if the  
464 optical background is properly removed. We compared the HCl profile retrievals  
465 using an ideal ILS with those using an actual measured ILS. The results showed that  
466 the total column amounts were under estimated by about 0.4% if a ME amplitude is  
467 deviated by about -3.5%. Furthermore, the retrieval errors increase and profile  
468 deviations are obviously shown in a height range with a high retrieval sensitivity.  
469 ILSs deduced from all scenarios of lamp cell measurements are compared, and are  
470 further used to derive HCl profile from the same spectrum. As a result, the influence



471 of different attenuators on the ILS of a high resolution FTIR spectrometer are  
472 quantified. The worst option to increase (decrease) the intensity is selecting a bigger  
473 (smaller) entrance aperture. This is because the mechanical errors of different  
474 apertures may be non-negligible and inconsistent. Inserting attenuators #1 ~ 4 before  
475 or behind the interferometer can be used to adapt the intensity of a detector. While  
476 inserting a grid-like attenuator #1 behind the interferometer is the optimum option. It  
477 can produce a scenario close to an ideal ILS assumption if the interferometer is  
478 already well aligned.

## 479 **8 Acknowledgements**

480 This work is jointly supported by Anhui Province Natural Science Foundation of  
481 China (Grant NO. 1308085QF124), the National Natural Science Foundation of China  
482 (Grants NO.41530644, NO.41571130023, NO. 41275038, NO.91544212 and NO.  
483 41575021), the e National Key Technology R&D Program of China  
484 (2014BAC22B00), the National High Technology Research and Development  
485 Program of China (2014AA06A508, 2014AA06A511), the Scientific and  
486 Technological Project of Anhui Province (1301022083), the Special Project of  
487 Environmental Nonprofit Industry Research China (201409006) and the German  
488 Federal Ministry of Education and Research (BMBF) (Grant NO. 01LG1214A). All  
489 experiments are accomplished in IUP, University of Bremen, all assistances and  
490 hospitalities from members of FTIR group, IUP are appreciated. The LINEFIT code is  
491 provided by Frank Hase, Karlsruhe Institute of Technology (KIT), Institute for  
492 Meteorology and Climate Research (IMK-ASF), Germany. The processing  
493 environment of SFIT4 and some plot programs are provided by Eric Nussbaumer,  
494 National Center for Atmospheric Research (NCAR), Boulder, Colorado, USA.

## 495 **9 References**

496 Angelbratt, J., Mellqvist, J., Blumenstock, T., Borsdorff, T., Brohede, S., Duchatelet,  
497 P., Forster, F., Hase, F., Mahieu, E., Murtagh, D., Petersen, A. K., Schneider, M.,  
498 Sussmann, R., and Urban, J.: A new method to detect long term trends of methane  
499 (CH<sub>4</sub>) and nitrous oxide (N<sub>2</sub>O) total columns measured within the NDACC  
500 ground-based high resolution solar FTIR network, Atmos. Chem. Phys., 11,



- 501 6167–6183, doi:10.5194/acp-11-6167-2011, 2011.
- 502 Davis, S. P., Abrams, M. C., and Brault, J. W.: Fourier transform spectrometry,  
503 Academic Press, ISBN: 0-12-042510-6, 2001.
- 504 Dohe, S., Sherlock, V., Hase, F., Gisi, M., Robinson, J., Sepúlveda, E., Schneider, M.,  
505 and Blumenstock, T.: A method to correct sampling ghosts in historic  
506 near-infrared Fourier transform spectrometer (FTS) measurements, Atmos. Meas.  
507 Tech., 6, 1981–1992, doi:10.5194/amt-6-1981-2013, 2013.
- 508 Dammers, E., Vigouroux, C., Palm, M., Mahieu, E., Warneke, T., Smale, D.,  
509 Langerock, B., Franco, B., Van Damme, M., Schaap, M., Notholt, J., and Erisman,  
510 J. W.: Retrieval of ammonia from ground-based FTIR solar spectra, Atmos. Chem.  
511 Phys., 15, 12789–12803, doi:10.5194/acp-15-12789-2015, 2015.
- 512 Griffith, D.: ILS sensitivity study by modulation-efficiency weighting of  
513 interferograms, Material presented on TCCON teleconference in January, 2010.
- 514 Hannigan, J. and Coffey, M.: semiautonomous FTS observation system for remote  
515 sensing of stratospheric and tropospheric gases, Journal of Atmospheric and  
516 Oceanic Technology . 09/2009; 26(9). DOI: 10.1175/2009JTECHA1230.1
- 517 Hase, F., Demoulin, P., Sauval, A., Toon, G. C., Bernath, P., Goldman, A., Hannigan, J.,  
518 Rinsland C.: An empirical line-by-line model for the infrared solar  
519 transmittance spectrum from 700 to 5000  $\text{cm}^{-1}$ , J. Quant. Spectrosc. Radiat.  
520 Transfer, 2006, 102, 450 - 463
- 521 Hase, F.: Improved instrumental line shape monitoring for the ground-based,  
522 high-resolution FTIR spectrometers of the Network for the Detection of  
523 Atmospheric Composition Change, Atmos. Meas. Tech., 5, 603–610,  
524 doi:10.5194/amt-5-603-2012,2012.
- 525 Hase, F., Drouin, B. J., Roehl, C. M., Toon, G. C., Wennberg, P. O., Wunch, D.,  
526 Blumenstock, T., Desmet, F., Feist, D. G., Heikkinen, P., De Mazière, M.,  
527 Rettinger, M., Robinson, J., Schneider, M., Sherlock, V., Sussmann, R., Té, Y.,  
528 Warneke, T., and Weinzierl, C.: Calibration of sealed HCl cells used for TCCON  
529 instrumental line shape monitoring, Atmos. Meas. Tech., 6, 3527–3537,  
530 doi:10.5194/amt-6-3527-2013, 2013.



- 531 Hase, F. and Blumenstock, T.: Alignment procedure for Bruker IFS 120 spectrometers,  
532 NDSC Infrared Working Group Meeting, Bordeaux, 2001.
- 533 Hase, F., Blumenstock, T., and Paton-Walsh, C.: Analysis of the instrumental line  
534 shape of high-resolution Fourier transform IR spectrometers with gas cell  
535 measurements and new retrieval software, *Appl. Optics*, 38, 3417–3422, 1999.
- 536 Keppel-Aleks, G., Wennberg, P. O., and Schneider, T.: Sources of variations in total  
537 column carbon dioxide, *Atmos. Chem. Phys.*, 11, 3581–3593,  
538 doi:10.5194/acp-11-3581-2011, 2011.
- 539 Kurylo, M. J.: Network for the detection of stratospheric change (NDSC), SPIE  
540 Proceedings 1991, *P. Soc. Photo-Opt. Ins.*, 1491, 168–174, 1991.
- 541 Kohlhepp, R., Barthlott, S., Blumenstock, T., Hase, H., Kaiser, I., Raffalski, U., and  
542 Ruhnke, R.: Trends of HCl, ClONO<sub>2</sub>, and HF column abundances from  
543 ground-based FTIR measurements in Kiruna (Sweden) in comparison with  
544 KASIMA model calculations, *Atmos. Chem. Phys.*, 11, 4669–4677, 2011  
545 www.atmos-chem-phys.net/11/4669/2011/doi:10.5194/acp-11-4669-2011
- 546 Messerschmidt, J., Macatangay, R., Notholt, J., Petri, C., Warneke, T., and Weinzierl,  
547 C.: Side by side measurements of CO<sub>2</sub> by ground-based Fourier transform  
548 spectrometry (FTS), *Tellus B*, 62, 749–758, doi:10.1111/j.1600-0889.2010.00491.x  
549 ,2010.
- 550 Miller, C. E., Crisp, D., DeCola, P. L., Olsen, S. C., Randerson, J. T., Michalak, A. M.,  
551 Alkhaled, A., Rayner, P., Jacob, D. J., Suntharalingam, P., Jones, D. B. A.,  
552 Denning, A. S., Nicholls, M. E., Doney, S. C., Pawson, S., Boesch, H., Connor, B.  
553 J., Fung, I. Y., O'Brien, D., Salawitch, R. J., Sander, S. P., Sen, B., Tans, P., Toon,  
554 G. C., Wennberg, P. O., Wofsy, S. C., Yung, Y. L., and Law, R. M.: Precision  
555 requirements for space-based X-CO<sub>2</sub> data, *J. Geophys. Res.-Atmos.*, 112,  
556 D10314, doi:10.1029/2006JD007659, 2007.
- 557 Notholt, J., Kuang Z., Rinsland C.P., Toon G.C., Rex M., Jones N., Albrecht T.,  
558 Deckelmann H., Krieg J., Weinzierl C., Bingemer H., Weller R., Schrems O.:  
559 Enhanced upper tropical tropospheric COS: Impact on the stratospheric aerosol  
560 layer, *Science*, 300, 307-310, 2003.



- 561 Olsen, S. C. and Randerson, J. T.: Differences between surface and column  
562 atmospheric CO<sub>2</sub> and implications for carbon cycle research, *J. Geophys.*  
563 *Res.-Atmos.*, 109, D02301, doi:10.1029/2003JD003968, 2004.
- 564 Palm, M., Melsheimer, C., Noël, S., Heise, S., Notholt, J., Burrows, J. and Schrems,  
565 O.: Integrated water vapor above Ny Alesund, Spitsbergen: a multisensor  
566 intercomparison. *Atmospheric Chemistry and Physics*, 10 (3). pp. 1215-1226,  
567 2010.
- 568 Rodgers, C. D.: *Inverse Methods for Atmospheric Sounding: Theory and Practice*,  
569 World Scientific Publishing Co., Singapore, 2000.
- 570 Schneider, M., Redondas, A., Hase, F., Guirado, C., Blumenstock, T., and Cuevas, E.:  
571 Comparison of ground-based Brewer and FTIR total column O<sub>3</sub> monitoring  
572 techniques, *Atmos. Chem. Phys.*, 8, 5535–5550, doi:10.5194/acp-8-5535-2008,  
573 2008.
- 574 Sussmann, R., Forster, F., Rettinger, M., and Jones, N.: Strategy for high accuracy  
575 and precision retrieval of atmospheric methane from the mid-infrared FTIR  
576 network, *Atmos. Meas. Tech.*, 4, 1943–1964, doi:10.5194/amt-4-1943-2011,  
577 2011.
- 578 Washenfelder, R. A.: Column abundances of carbon dioxide and methane retrieved  
579 from ground-based near-infrared solar spectra, PhD thesis, California Institute of  
580 Technology, Pasadena, California (available at: <http://thesis.library.caltech.edu>),  
581 2006.
- 582 Wang, Y., Deutscher, N. M., Palm, M., Warneke, T., Notholt, J., Baker, I., Berry, J.,  
583 Suntharalingam, P., Jones, N., Mahieu, E., Lejeune, B., Hannigan, J., Conway, S.,  
584 Mendonca, J., Strong, K., Campbell, J. E., Wolf, A., and Kremser, S.: Towards  
585 understanding the variability in biospheric CO<sub>2</sub> fluxes: using FTIR spectrometry  
586 and a chemical transport model to investigate the sources and sinks of carbonyl  
587 sulfide and its link to CO<sub>2</sub>, *Atmos. Chem. Phys.*, 16, 2123-2138, doi:10.5194/acp  
588 -16-2123-2016, 2016.
- 589 Warneke, T., Petersen, A. K., Gerbig, C., Jordan, A., Rödenbeck, C., Rothe, M.,  
590 Macatangay, R., Notholt, J., and Schrems, O.: Co-located column and in situ



591 measurements of CO<sub>2</sub> in the tropics compared with model simulations, Atmos.  
592 Chem. Phys., 10, 5593-5599, doi:10.5194/acp-10-5593-2010, 2010.

593 Wunch, D., Toon, G. C., Wennberg, P. O., Wofsy, S. C., Stephens, B. B., Fischer, M.  
594 L., Uchino, O., Abshire, J. B., Bernath, P., Biraud, S. C., Blavier, J.-F. L., Boone,  
595 C., Bowman, K. P., Browell, E. V., Campos, T., Connor, B. J., Daube, B. C.,  
596 Deutscher, N. M., Diao, M., Elkins, J. W., Gerbig, C., Gottlieb, E., Griffith, D.  
597 W. T., Hurst, D. F., Jiménez, R., Keppel-Aleks, G., Kort, E. A., Macatangay, R.,  
598 Machida, T., Matsueda, H., Moore, F., Morino, I., Park, S., Robinson, J., Roehl, C.  
599 M., Sawa, Y., Sherlock, V., Sweeney, C., Tanaka, T., and Zondlo, M. A.:  
600 Calibration of the Total Carbon Column Observing Network using aircraft profile  
601 data, Atmos. Meas. Tech., 3, 1351–1362, doi:10.5194/amt-3-1351-2010, 2010.

602 Wunch, D., Toon, G. C., Blavier, J.-F. L., Washenfelder, R., Notholt, J., Connor, B. J.,  
603 Griffith, D. W. T., Sherlock, V., and Wennberg, P. O.: The Total Carbon Column  
604 Observing Network, Phil. T. Roy. Soc. A, 369, 2087–2112, doi:10.1098  
605 /rsta.2010.0240, 2011.

606 Wunch, D., Toon G. C., Sherlock V., Deutscher N. M., Liu C., Feist D. G., and  
607 Wennberg P. O.: The Total Carbon Column Observing Network's GGG2014 Data  
608 Version. 10.14291/tccon.ggg2014.documentation.R0/1221662.